available at www.sciencedirect.com

ScienceDirect

journal homepage: www.elsevier.com/locate/jmbbm

Research paper

The effect of poly (L-lactic acid) nanofiber orientation on osteogenic responses of human osteoblast-like MG63 cells

Bo Wang[a,c], Qing Cai[b], Shen Zhang[b], Xiaoping Yang[b,], Xuliang Deng[a,c,**]*

[a] *Department of Geriatric Dentistry, Peking University School and Hospital of Stomatology, Beijing 100081, PR China*
[b] *Key Laboratory of Carbon Fiber and Functional Polymers, Ministry of Education, College of Materials Science and Engineering, Beijing University of Chemical Technology, Beijing 100029, PR China*
[c] *Center for Biomedical Materials and Tissue Engineering, Academy for Advanced Interdisciplinary Studies, Peking University, Beijing 100871, PR China*

ARTICLE INFO

ABSTRACT

In this study, poly (L-lactic acid) (PLLA)/trifluoroethanol (TFE) solution was electrospun to fabricate fibrous scaffolds with different fiber orientations. Random and parallel PLLA nanofiber alignments were achieved by using a metal plate and a rolling rod as the receiver, respectively. The parallel PLLA fibrous scaffolds were further hot-stretched to obtain hyperparallel PLLA fibrous scaffolds. The PLLA fibrous scaffolds were characterized by fiber diameter, interfiber distance, fiber array angle, water contact angle, morphology and mechanical strength. The tensile strength of hyperparallel nano-fibers was approximately 5- and 14-times the parallel and random fibers, respectively. Osteoblast-like MG63 cells were cultured on the PLLA scaffolds to study the effects of fiber orientation on cell morphology, proliferation and differentiation. The cells on the randomly-oriented scaffolds showed irregular forms, while the cells exhibited shuttle-like shapes on the parallel scaffolds and had larger aspect ratios along the fiber direction of the hyperparallel scaffolds. Alkaline phosphatase (ALP) activity and collagen I (placeStateCol I) and osteocalcin (OC) deposition exhibited fiber orientation dependence. With an increase in parallelism of the fibers, there was a decrease in ALP activity and placeStateCol I and OC production. These results suggest that exploitation of PLLA fiber orientation may be used to control osteoblast-like cell responses.

1. Introduction

The current challenge in bone tissue engineering is to fabricate a bioartificial bone graft mimicking the extracellular matrix (ECM) with effective bone mineralization, resulting in the regeneration of fractured or diseased bones. In numerous studies, cells have been reported able to sense micro and nanoscale geometric cues from their environments through the phenomenon of contact guidance. The interactions

---

* *Corresponding author.* Tel.: +86 10 64412084; fax: +86 10 64412084.
** *Corresponding address:* Department of VIP Dental Service, School and Hospital of Stomatology, Peking University, Beijing 100081, PR China. Tel.: +86 10 62173410; fax: +86 10 62179977 5581.
E-mail addresses: yangxp@mail.buct.edu.cn (X. Yang), kqdxl@bjmu.edu.cn (X. Deng).

between the cells and the topographically different substrates lead to specific cell responses and result in different cell functions (Guilak et al., 2009).

Electrospinning has been a popular technique to produce fibrous scaffolds for tissue engineering, for its simplicity in mimicking the features of natural extracellular matrix (Sundaray et al., 2006). Fibrous scaffolds with different topographical features can be readily obtained by adjusting fiber diameter, alignment and interfiber distance (He et al., 2010). Effects of fiber diameter and alignment on spreading, proliferation, and differentiation of various cells, such as fibroblasts (Gregory et al., 2009; Liu et al., 2009; Lowery et al., 2010), meniscal fibrochondrocytes (Baker and Mauck, 2007), osteoblastic cells (Badami et al., 2006), human mesenchymal stem cells (Lorenzo et al., 2006; Baker et al., 2010), Schwann cell and neural stem cells (We et al. 2009; Christopherson et al., 2009) etc., have been intensively studied and published. Fiber-alignment was found playing an important role in directing cell orientation, augmenting matrix content and organization, and promoting cell differentiation.

As for bone tissue engineering, some researchers have identified that random nanofibrous scaffolds were favorable for the osteogenesis of bone marrow mesenchymal stem cells (Li et al., 2006) and stimulating bone formation (Khang et al., 2006; Kim et al., 2008; Li et al., 2006). The results suggest that random nanofibrous scaffolds can partially possess topographic features and biological functions to native bone ECM (Barnes et al., 2007; Woo et al., 2007).

Bone tissue is a kind of collagen-rich tissue composed of certain parallel-arranged collagen fibers. Linear parallel raised features, e.g. microgrooves, with length scales of 0.5–2 μm have been shown to enhance alkaline phosphatase (ALP) activity and mineral deposition (Matsuzaka et al., 1999; Zhu et al., 2005; Zinger et al., 2005). Therefore, the parallel nanofibrous scaffolds theoretically presented a suitable foundation for engineering of bone tissues. However, sparse research can be found concerning the effect of parallel fiber orientation on the specific osteogenic differentiation.

To determine the effects of nanotopography on the differentiation of osteoblastic cells and develop a biomimetic scaffold for bone tissue engineering, in the present study, PLLA nanofibrous scaffolds with random or parallel fiber orientation were prepared by using electrospinning. Besides, parallel PLLA nanofibrous scaffold was further hot-stretched to produce a kind of hyperparallel-aligned PLLA nanofibrous scaffold. All the nanofibrous scaffolds were characterized in terms of fiber diameter, interfiber distance, morphology and mechanical properties. The effects of fiber orientation on cell adhesion, morphology, proliferation and differentiation of osteoblast-like MG63 cells were examined.

2. Materials and methods

2.1. Materials

Reagents used in this study included the following: PLLA ($M_w = 10 \times 10^4$, Institute of Shan Dong Biomedical Instruments, China), dimethyl sulfoxide (DMSO, Sigma, USA),
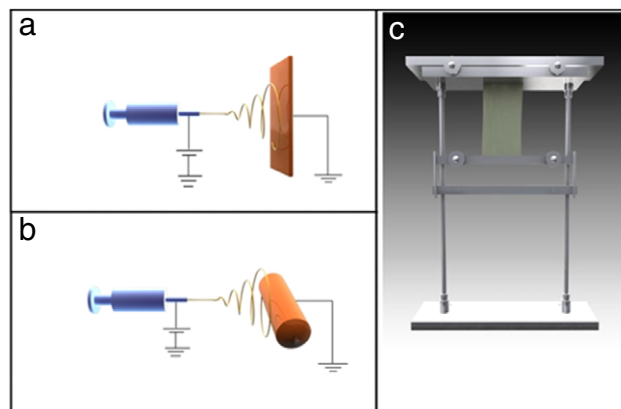

Fig. 1 – Schematic diagram of electrospun PLLA nanofibrous scaffold devices: (a) a metal plate as a collector, (b) a rolling rod as a collector; (c) hot-stretch device.

Dulbecco's modified Eagle's medium (DMEM, Gibco, USA), fetal bovine serum (FBS, Gibco, USA), penicillin (Gibco, USA), streptomycin (Gibco, USA), trypsinase (Sigma, USA), ethylene diamine tetraacetic acid (EDTA, Sigma, USA), WST-1 (cell proliferation and cytotoxicity assay kit, Bi Yun Tian, China), Type I collagen (Col I, CICP, Prolagen-Cenzyme Immunoassay Kit, Metra Biosystem, CA, USA), Alkaline phosphatase (ALP, Sigma Kinetic Method Kit, St. Louis, MO, USA) and Osteocalcin (OC, Novocalcin Enzyme Immunoassay Kit, Metra Biosystem).

2.2. Electrospun PLLA nano-fibers with different orientations

A polymer solution was prepared by dissolving 0.7 g of PLLA powders in 10 ml TFE and stirred overnight. The solution was electrospun from a 20 ml syringe with a steel needle (inner diameter of 0.5 mm) at a rate of 0.7 ml/h continuously with a programmable syringe pump (Top 5300, Japan). A voltage (15 kV) was applied to the tip of the needle by the use of a high-voltage supply (DW-P303-1AC, China) when a fluid jet was ejected. To obtain randomly arranged PLLA nano-fibrous scaffolds, a metal plate (20×25 cm^2) was used as a collector at a distance of 18-cm from the tip of the needle. To obtain parallel PLLA nanofibrous scaffolds, a cylindrical drum, which rotated at a surface linear rate of 12 m/s, was used as a collector at a distance of 18 cm from the tip of the needle. To achieve hyperparallel PLLA nano-fibrous scaffolds, parallel PLLA nano-fibrous scaffolds were cut into 6 cm in length along the fiber orientation and 5 cm in width. The membrane was fixed on the stretching set as shown in Fig. 1(c) and drawn by using 300 g weight at 100 °C for 5 min along the fiber axial direction. Before cell culture, all PLLA nano-fibrous scaffolds were exposed to a vacuum oven (DZF-6210, Bluepard, China) at room temperature for 2 weeks to remove residual solvent.

2.3. Characterization of electrospun PLLA scaffolds

The morphologies of electrospun PLLA nano-fibrous scaffolds were studied by scanning electron microscopy (SEM) (Top 5300, Japan) with an accelerating voltage of 15 kV. Before the observation, the scaffolds were coated with gold using

a sputter coater (Jeol JFC-1200 Fine Coater, Japan). The fiber diameter, interfiber distance and fiber arrangement were measured from the SEM photographs using image analysis software (Image J, National Institutes of Health, USA). PLLA nano-fibrous scaffolds were carefully cut into rectangles ($4 \times 20 \times 0.05$ mm³) and a tensile test was conducted by an Instron (Model 1121) at a 20 mm/min crosshead speed with a 10 mm gauge length at room temperature. The tensile stress of each scaffold was calculated from the nominal cross-sectional area of the tensile specimen (Gang et al., 2007). Static water contact angles of the electrospun scaffolds were measured by a Cam 200 Optical Contact Angle Meter (KSV Instruments, Monroe, CT, USA), equipped with a CCD camera (KGV-5000, USA). Briefly, the electrospun scaffolds were attached to a silicon wafer. Approximately 5 μl of distilled water was pipetted onto the membrane. Temporal images of the droplet were taken after 5 s. The contact angles were calculated by computer analysis of the acquired images. The chosen experimental conditions were at 25 °C and 65% humidity. The crystallinity of random, parallel and hyperparallel PLLA scaffolds was investigated using X-ray diffraction (XRD, Rigaku D/max 2500 VB2+/PC, Japan).

2.4. Cell culture and seeding on PLLA nano-fibrous scaffolds

MG63 human osteoblast-like cells were cultured in DMM supplemented with 10% FBS and antibiotics (100 u ml⁻¹ penicillin and 100 mg ml⁻¹ streptomycin). The cells were detached from culture flasks by trypsinization and centrifuged. Prior to cell seeding, all PLLA nano-fibrous scaffolds were cut into 1.3×1.3 cm², placed into 24-well plates, sterilized with ultraviolet (UV) light for 1 h, immersed in 70% ethanol for 10 min, followed by washing three times with phosphate-buffered saline (PBS) solution. Each cell suspension (1 ml) was plated at a density of 2×10^4 cells ml⁻¹ in the 24-well plates containing sterile samples of PLLA nano-fibrous scaffolds for the cell attachment assays. Cell suspensions (200 μl) were plated at a density of 2×10^4 cells ml⁻¹ in the 24-well plates containing sterile samples of the scaffolds for the proliferation, morphology and differentiation studies. Cell suspensions added into wells containing no materials were regarded as controls (tissue culture plates, TCPs). Plates were cultured in standard conditions at 37 °C, 95% humidity and 5% CO_2. After 24 h, the medium was replaced with DMEM supplemented with β-glycerophosphate (1×10^{-8} nM) and ascorbic acid (50 μg/ml) to stimulate osteogenesis. The medium was changed every two days. To stimulate the production of OC, the culture medium was enriched with $1, 25(OH)_2D3$ 48 h before the end of the experiment.

2.5. Attachment and proliferation of cells on PLLA nano-fibrous scaffolds

After incubating the plates for 6 h, the adherent cells were removed by trypsinization, and live cells were stained with an equal volume of 0.2% trypan blue solution. Finally, the viable cells were enumerated using a hemocytometer under a light microscope. The experiment was repeated three times. At 1, 3, 5 and 7 days of culture, cell proliferation and viability were assessed using a Cell Proliferation Reagent WST-1 test. The WST-1 solution (100 μl) and medium (900 μl, final dilution: 1:10) were added to each plate. The multi-well plates were incubated at 37 °C for an additional 4 h, and supernatants were quantified spectrophotometrically at 450 nm with a reference wavelength of 640 nm. Results of the WST-1 were reported as optical density (OD).

2.6. Morphology of cells on nano-fibrous scaffolds

SEM micrographs were taken at 1 and 2 days following the initial cell-seeding on the scaffolds. Briefly, the co-cultured constructs were harvested, washed with PBS and then fixed with 4% glutaraldehyde. Following 3 rinses with water, the samples were dehydrated through a series of graded alcohol solutions and then air-dried overnight. Dry cellular constructs were sputter coated with gold and observed by SEM at an accelerating voltage of 15 kV (Top 5300, Japan).

2.7. Cytoskeleton of cells on nano-fibrous scaffolds

After 48 h culture, constructs were washed with PBS, fixed for 5 min in 3.7% formaldehyde in PBS, then washed extensively with PBS, permeabilized with 0.1% Triton X-100 in PBS and washed again in PBS. Cells were stained with a 50 ug/ml fluorescent phalloidin-conjugate solution in PBS (containing 1% DMSO from the original stock solution) for 40 min at room temperature and then washed several times with PBS to remove unbound phalloidin-conjugate. Laser scanning confocal microscopy (LSCM) (TCS SP2, Leica, Germany) was applied to observe the samples.

2.8. Differentiation of cells on PLLA nano-fibrous scaffolds

The levels of COL I, ALP activity and OC present in co-culture supernatants were determined by ELISA, following the manufacturer's instructions. Briefly, at culture times of 7, 14 and 21 days, the supernatant was collected from each well and centrifuged to remove particulates, if any. Aliquots were dispensed in Eppendorf tubes for storage at −70 °C. After standards and samples were added into each 96-well plate pre-coated with antigen, the first antibody was added into each well and incubated for 30 min at 37 °C. After aspirating and washing 5 times, the second antibody was added into each well and incubated for 30 min at 37 °C. Following aspiration and 5 washes, tetramethylbenzidine was added into each well and incubated for 20 min at room temperature. A stop solution was added into each well, and the absorbance value was read by a microplate reader at a 450 nm wavelength within 15 min. The measured concentration and activity were normalized by cell number to take into account the differences in cell growth (Boanini et al., 2006).

2.9. Statistical analysis

Statistical analysis was performed using an SPSS 10 statistical package, and values were considered significant at $p < 0.05$. The Student's t-test was used to compare the data from the experimental and control samples.
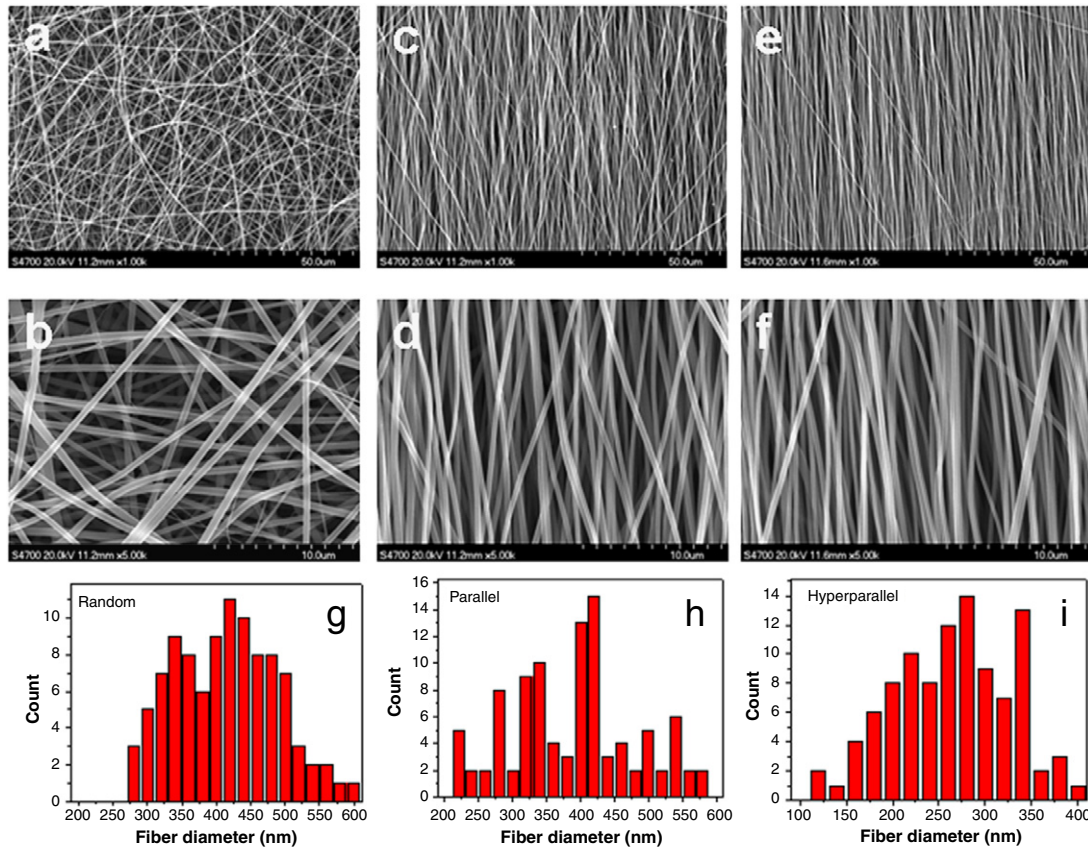
Fig. 2 – Scanning electron microscopy (SEM) photomicrographs and fiber diameter distribution of the three electrospun PLLA nanofibrous scaffolds with different fiber arrangements: (a, b, G) random; (c, d, H) parallel-aligned; (e, f, I) hyperparallel-aligned.

Table 1 – Properties of the three types of electrospun PLLA nanofibrous scaffolds prepared in this study.						
Group	Fiber diameter (nm)	Fiber distance (μm)	Water contact angle (°)	Water contact angle (after ethanol treated)	Tensile strength (MPa)	Tensile modulus (MPa)
Random	450 ± 50	$2.2 \pm 0.4-$	144.2 ± 0.7	21.2 ± 2.32	8.32 ± 1.56	230.355 ± 40.454
Parallel-aligned	325 ± 75	1.6 ± 0.3	132.1 ± 0.5	18.5 ± 1.73	21.56 ± 2.07	409.7 ± 44.20
Hyperparallel-aligned	275 ± 25	1.0 ± 0.2	107.5 ± 0.8	13.1 ± 1.21	117.02 ± 4.58	1122.84 ± 98.74
Tensile data are expressed as means $\pm$ SD, $n = 10$.						

3. Results

3.1. Fiber morphology, diameter and array angle of PLLA nano-fibrous scaffolds

As shown in Fig. 2, all of the fibers demonstrated uniformly smooth surfaces. The random PLLA nano-fibers showed isotropic fiber alignments. The parallel and hyperparallel PLLA fibers exhibited anisotropic alignments. The hyperparallel group showed a higher order of fiber arrangement than the parallel group.

Fiber diameter distribution analysis is shown in Fig. 2(g)–(i) and Table 1. The diameters of the randomly aligned fibers were in the range of 450±50 nm. The diameters of the parallel fibers decreased to 325 ± 75 nm, and that of the hyperparallel fibers resulting from hot-stretching further lowered to 275 ± 25 nm. The interfiber distances of the random, parallel and hyperparallel scaffolds were 2.2 ± 0.4 μm, 1.6 ± 0.3 μm and 1.0 ± 0.2 μm, respectively, as shown in Table 1.

The fiber arrangement evaluated with Image J software is demonstrated in Fig. 3. The fibers in the random group were deposited in all directions. The fibers in the parallel group were oriented between $-40°$ and $+45°$. More than 46% of the
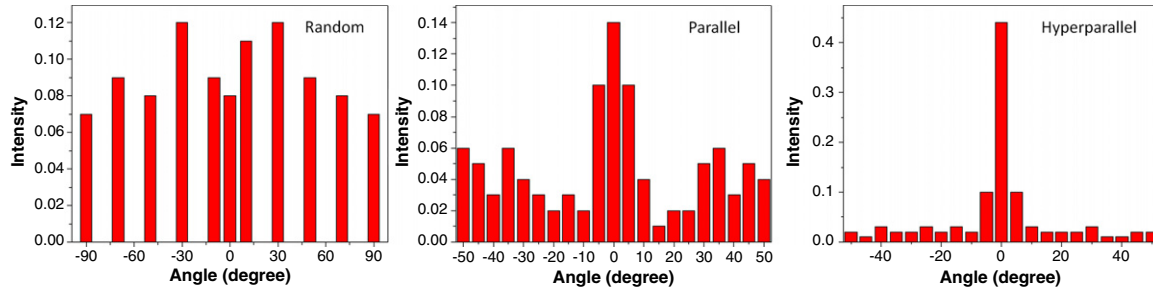
Fig. 3 – Assessment of fiber angle in random-, parallel- and hyperparallel-aligned PLLA nanofibrous scaffolds.
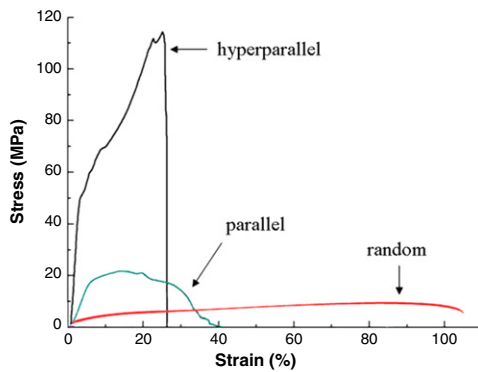

Fig. 4 – Typical tensile stress–strain curves of PLLA nanofibrous scaffolds with different fiber orientations.

fibers in the hyperparallel PLLA nano-fibrous scaffolds were found in the orientation of 0°.

3.2.   Contact angle of PLLA nano-fibrous scaffolds

From the data presented in Table 1, the water contact angles of the random and parallel PLLA nano-fibrous scaffolds were much higher than that of the hyperparallel group. The water contact angles of the PLLA nano-fibrous scaffolds were 144.2± 3.7°, 132.1°±2.5° and 107.5°±3.8° for the random, parallel and hyperparallel alignments, respectively.

3.3.   Tensile strength of PLLA nano-fibrous scaffolds

The tensile strength–strain curves obtained from the PLLA nano-fibrous scaffolds with random, parallel and hyperparallel topographies are shown in Fig. 4, and the mechanical properties of the scaffolds are summarized in Table 1. As the fiber orientation increased, the PLLA nano-fibrous scaffolds showed a significantly increased tensile strength and modulus. The tensile strength of the hyperparallel PLLA nano-fibrous scaffolds increased to 117.02 MPa rapidly under extension until 27.6% of strain, much higher than that of the parallel group at 21.56 MPa within 40% of strain and that of the random group at 8.32 MPa within 101% of strain.

3.4.   Crystallinity of PLLA nano-fibrous scaffolds

XRD analysis in Fig. 5 demonstrates that the as-spun PLLA samples (random and parallel) did not exhibit a crystalline
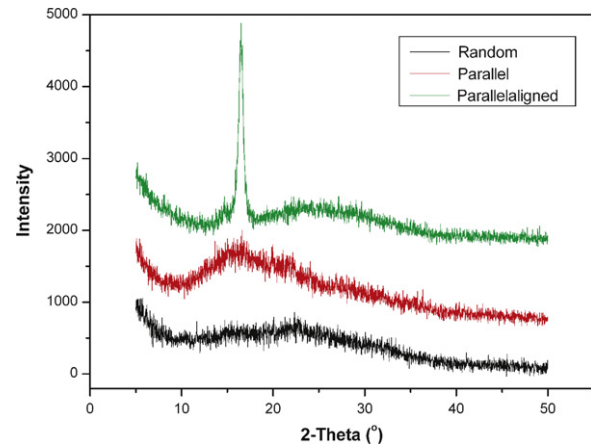

Fig. 5 – Representative X-ray diffraction (XRD) patterns of PLLA nanofibrous scaffolds with different fiber orientations.

nature, although PLLA is considered a type of semi-crystalline polyester polymer. After being hot-stretched 100%, a sharp peak at 16° could be detected in the hyperparallel PLLA nano-fibers, corresponding to the occurrence of PLLA crystallization.

3.5.   Attachment and proliferation of MG63 cells on PLLA nano-fibrous scaffolds

The numbers of osteoblast-like cells adherent to the PLLA nano-fibrous scaffolds and TCP are shown in Fig. 6. The cells on the random PLLA nano-fibrous scaffolds (1.68×10^4) were higher in number than those quantified on the parallel-oriented scaffolds (1.64×10^4) and TCP (1.5×10^4), but not significantly different at the 6 h time point. The number of adherent cells on the hyperparallel PLLA nano-fibrous scaffolds (1.62×10^4) was lower than the cell numbers on the random (1.68×10^4) and parallel (1.64×10^4) scaffolds at 6 h.

The proliferation rates of MG63 cells on PLLA nano-fibrous scaffolds are shown in Fig. 7. Cell density increased from day 1 through day 7 in all groups, although there was no statistical difference among the random and parallel scaffolds and TCP group. The hyperparallel group exhibited a significantly lower cell density than the other groups.
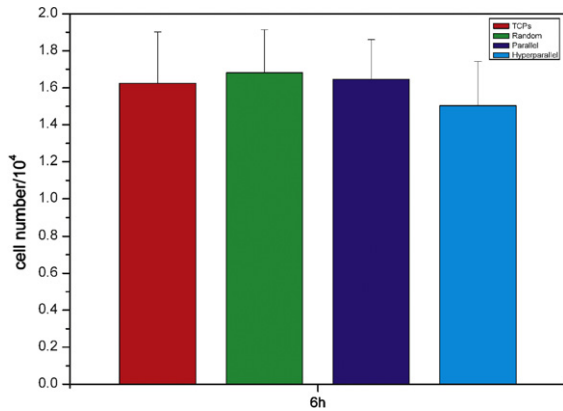
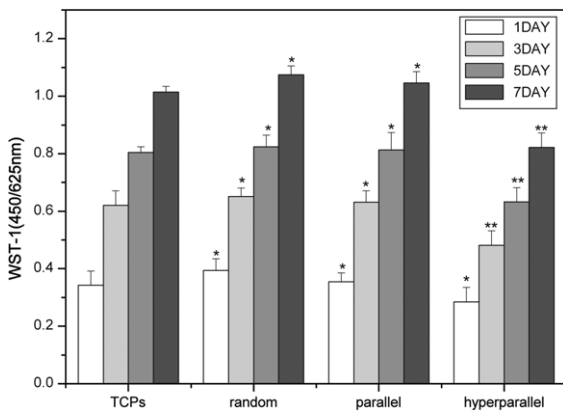**Fig. 6 – MG63 cells attached on random-, parallel- and hyperparallel-aligned PLLA nanofibrous scaffolds.**

Fig. 7 – MG63 cell proliferation after 1, 3, 5 and 7 days of culture on nanofibrous scaffolds with different topographies (*$p < 0.05$; ** $p < 0.005$).

3.6.   Morphology of MG63 cells on PLLA nano-fibrous scaffolds

The morphology of MG63 cells cultured on PLLA nano-fibrous scaffolds with random, parallel and hyperparallel topographies are shown in Fig. 8. For all PLLA scaffolds, MG63 cells adhered and grew well, and the cells appeared to interact and associate with the surrounding fibers. The MG63 cells cultured on the random PLLA nano-fibrous scaffolds showed polygonal forms with no obvious orientations (Fig. 8(a), (b)). While on both parallel and hyperparallel scaffolds, the cells showed polarized forms with orientations along the fiber directions (Fig. 8(c)–(f′)). Notably, it could be seen that more filopodia-like extensions and filament-like structures extended from the MG63 cells on the random PLLA fibers than on the parallel and hyperparallel fibers (Fig. 8(b)′, (d)′, f′).

As seen in the LSCM images (Fig. 9), cells in the TCP group exhibited wide spreading of cellular actin filaments. As expected, the cellular actin filaments were primarily directionally-orientated on hyperparallel fibers, and showed the least organization on the random fibers (Fig. 9(b), (d)).

•The quantitative analysis of cellular polarity was expressed as an average aspect ratio (i.e. the ratio of the long axis to the short axis of the elliptical body) of the MG63 cells (Fig. 10(a)). The average aspect ratios of cells on the random, parallel and hyperparallel scaffolds were 2.34, 5.12 and 7.56, respectively. It was also found that the nuclei presented certain polarities along the fiber alignments (Fig. 9). On the hyperparallel PLLA nano-fibrous scaffolds, the nuclei appeared in mostly elongated shapes, while on the parallel scaffolds, the nuclei showed slightly elongated shapes. On the random fibers, most of the nuclei were elliptical in shape. The values of the nuclei average aspect ratios on random, parallel and hyperparallel scaffolds were 2.15, 3.23 and 4.24, respectively (Fig. 10(b)).

3.7.   Differentiation of MG63 cells on PLLA nano-fibrous scaffolds

The ALP activity in all groups increased from 7 to 14 days (Fig. 11(a)). From 14 to 21 days, the ALP activity of all groups slightly decreased. The hyperparallel group showed the lowest ALP activity, while the random and parallel scaffold groups showed higher ALP activities than the control group at 7, 14 and 21 days. Although the ALP activity was marginally higher in the random group than in the parallel group, the difference was not statistically significant.

At the 7th day, the production of Col I in all groups was the highest Fig. 11(b). As time increased to 14 days, the production decreased. By day 21, Col I production reached the lowest value in this experiment. At all three time points, the production of Col I in the hyperparallel group was the lowest, and the random and parallel groups exhibited higher Col I production than the TCP group. Although Col I production was higher in the random group than in the parallel group, the difference was not statistically significant.

At all experimental time points, the hyperparallel group exhibited the lowest OC production, and the random and parallel groups showed more OC production than the TCP group. At 14 days, the production of OC reached the highest level in all groups, and at 21 days, OC production decreased even under the level found at 7 days. Although OC secretion was minimally higher in the random group than in the parallel group at all time points, the difference was not statistically significant.

4.   Discussion

In previous studies, nano-fibrous scaffolds fabricated by electrospinning have been shown to be excellent tissue scaffolds for tissue regeneration (Wutticharoenmongkol et al., 2007; Schnell et al., 2007; Sangsanoh et al., 2007; Chen et al., 2007). Fiber diameter has been considered a parameter to regulate the cellular response to nano-fibers with multiple components (Bashur et al., 2006; Chen et al., 2007; Moroni et al., 2006). However, there are few reports regarding the effects of different fiber orientations on osteoblast differentiation of osteogenic progenitor cells.

In order to explore the effects of fiber orientation on the osteogenic differentiation of osteoblasts, in this work, random- and parallel-aligned PLLA nano-fibrous scaffolds were fabricated by an electrospinning technique. The randomly arranged fibers were obtained by using a metal plate as a collector (Doshi and Reneker, 1995). When a rolling rod is used as a
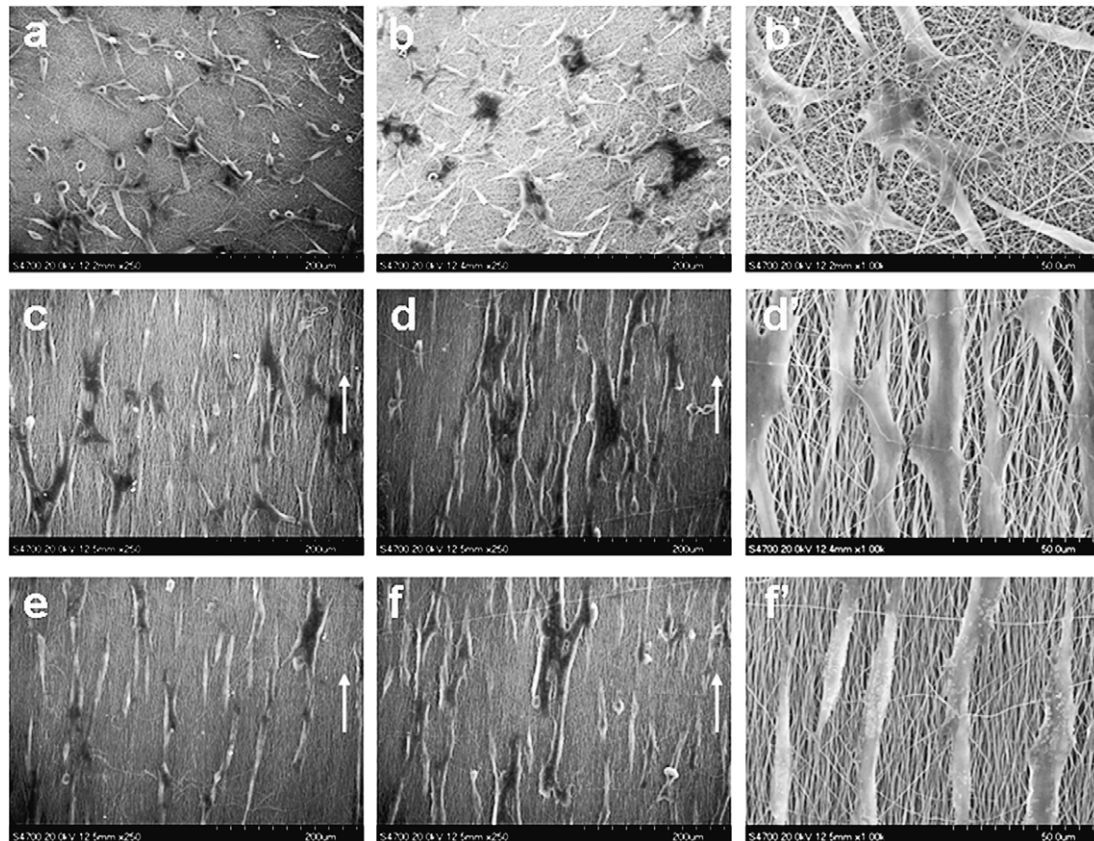
Fig. 8 – SEM images of MG63 cells cultured on PLLA nanofibrous scaffolds with different surface topographies: (a) random, 1 day; (b) random 2 days; (c) parallel-aligned, 1 day; (d) parallel-aligned, 2 days; (e) hyperparallel-aligned, 1 day; (f) hyperparallel-aligned, 2 days. Images (b′), (d′) and (f′) are higher magnification images of (b), (d) and (f′).
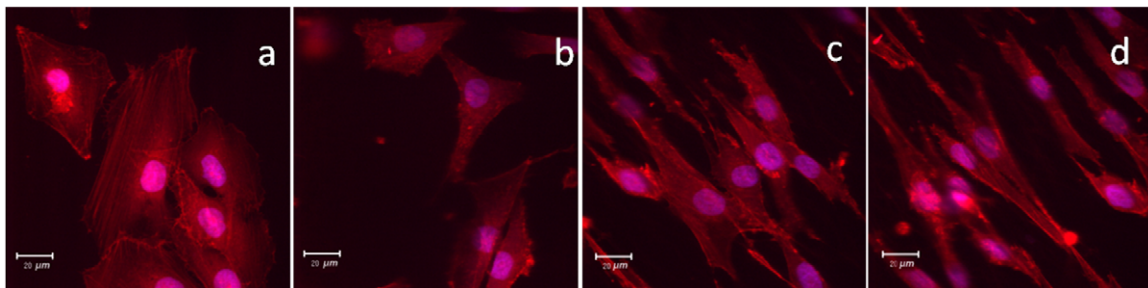

Fig. 9 – Laser scanning confocal microscopy (LSCM) micrographs of immunostained a-actin filaments in MG63 cells after 1 day of culture. Cell actin (green) and nuclei (red) were stained in cells cultured on (a) TCP; (b) random; (c) parallel-aligned; (d) hyperparallel-aligned scaffolds. (For interpretation of the references to colour in this figure legend, the reader is referred to the web version of this article.)

collector, because the edge of the rod collector exerts a pulling force on the jet, which stretches the collected nano-fibers and consequently increases the degree of fiber orientation and reduces the diameter of the resultant fibers (Katta et al., 2004). To obtain hyperparallel scaffolds, parallel-aligned PLLA fibers were further hot-stretched at 100 °C. The pulling force along the fiber axis further increased the degree of fiber orientation (Li et al., 2003). Fiber diameter and interfiber distance were found gradually decreasing from the random to parallel to hyperparallel groups. This finding is most likely due to the fact that the polymer jet was oriented with a non-linear trajectory.

The hyperparallel-aligned PLLA nano-fibrous scaffolds had the lowest water contact angle. The fibers with highest orientation in the hyperparallel-aligned PLLA scaffolds may support greater spreading of the water drop due to the effect of capillary absorption.

The hyperparallel-aligned fibers showed significant mechanical strength and occurrence of PLLA crystallization. We speculate that such an abrupt improvement of mechanical properties of the hyperparallel-aligned PLLA nano-fibers was mainly due to the increase of fiber crystallinity. As the electrospinning procedure was performed under room tem-
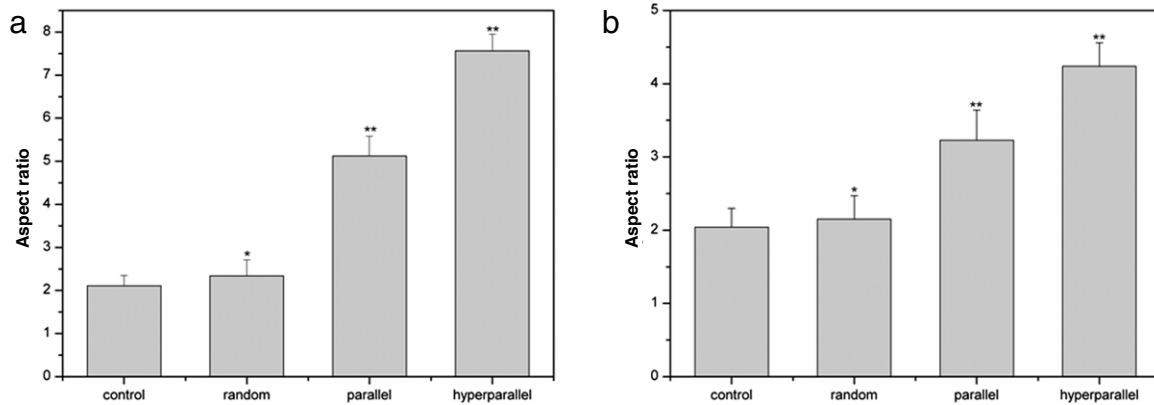
Fig. 10 – Aspect ratio of MG63 (a) cells and (b) nucleus on on nano-fibrous scaffolds with different topographies and on TCP after 24 h of culture ($*p < 0.05$; $**p < 0.005$).

perature, the inside of the PLLA chains in the as-spun nano-fibers did not crystallize during the fast fiber formation. Although fast rolling collection can increase fiber parallelism and density, this technique cannot increase fiber crystallinity. Thus, results in this work showed that the tensile strength of the parallel PLLA nano-fibrous membrane was not much higher than the random nano-fibrous scaffold. During the hot-stretch treatment, the PLLA chains re-arrange to form highly regular α-type crystalline structures (Zong et al., 2002; Ling and Spruiell, 2006). As a result, the tensile strength of the hyperparallel-aligned PLLA nano-fibrous membrane increased greatly.

By using the random, parallel and hyperparallel PLLA nanofibrous scaffolds, the cell phenotypic influences and osteogenic effects of PLLA fiber alignment on osteoblast-like MG63 cells were investigated. At first, the number of MG63 cells adhered to the hyperparallel-aligned PLLA nano-fibrous scaffolds was detected the least among the three PLLA scaffolds (Fig. 8). On the contrary, the adherence of MG63 cells was enhanced on the random and parallel PLLA nano-fibrous scaffolds (Fig. 6). Hydrophobic surfaces have been found more favorable for cell attachment than hydrophilic surfaces (Arima and Iwata, 2007). In agreement, the difference in the numbers of adhered cells was attributed to the water contact angles of the scaffolds.

The MG63 cells seeded on the PLLA scaffolds grew with an increase in culture time, however, the growth rates differed with the varied fiber alignments. We found that the random and parallel PLLA nano-fibrous scaffolds favored the proliferation of MG63 cells, while the hyperparallel PLLA nano-fibrous scaffolds supported a reduction in cell growth rates (Fig. 8). One possible explanation for this result is related to the porosity of the scaffold. In previous studies, Badami et al. presumed that mesh size was determined by the fiber diameter, and that large diameter fibers facilitated a better supply of oxygen, nutrients and tissue formation, on the contrary, small diameter fibers resulted in smaller pores, inhibited nutrient infiltration and limited further activities of cells (Badami et al., 2006). Consistent with previous studies, the results presented in Table 1 and Fig. 2 show that random and parallel PLLA nano-fibrous scaffolds provided more space for cell infiltration and growth than the densely packed

hyperparallel-aligned PLLA nano-fibers. Especially on the random PLLA nano-fibrous scaffolds, which had a relatively larger pore size and a looser fiber deposition, the cells could easily infiltrate the scaffold.

The cell and nucleus morphology of osteoblast-like MG63 cells had been greatly affected by fiber orientation, because the aspect ratio of each was found increasing with fiber orientation increasing. Flat and polygonal cells could be seen on random PLLA nano-fibrous scaffolds and TCP, while elongated and directionally-orientated cells were detected along the fiber direction of both parallel- and hyperparallel-aligned PLLA nano-fibers (Figs. 5 and 6). The contact guidance theory can support the observed relationship of cell and nuclei morphology between fiber arrangements, such that substrates with specific topographical features have been shown to induce cell alignment and migration through adhesion–cytoskeleton interactions according to the definite topography of the substrates (Chew et al., 2008). Because the fibers were thinner, denser and more parallel in the parallel and hyperparallel PLLA nano-fibrous scaffolds, the fibers contributed to larger aspect ratios in MG63 cell and nucleus shape in comparison with the randomly-aligned fibers in the random PLLA nano-fibrous scaffolds. Cell morphology is considered an important regulator for cell growth and differentiation. Indeed, the variations of cell shape and cytoskeleton tension affect the proliferation and differentiation of cells (Chen et al., 1997; Watt et al., 1988; Roskelley et al., 1994). The guidance of filopodia by nano-fibers and subsequent changes in cytoskeletal arrangements and signaling can alter mechanical forces within the cell (Mammoto and Ingber, 2010). Thus, it can be presumed that the elongated cytoskeleton resulting from the hyperparallel-aligned nano-fibers may affect interphase nucleus organization and genomic regulation.

In order to investigate the effect of cell shape on osteogenic differentiation, we evaluated the activity of ALP and the production of Col I and OC of osteoblast-like MG63 cells on the PLLA nano-fibrous scaffolds. ALP activity is an early marker of osteoblastic differentiation, and the increased expression of ALP may affect the progressive differentiation of cultured osteoblasts (Malaval et al., 1999). Col I is secreted by cells as a major component of the ECM (Malaval et al., 1999),
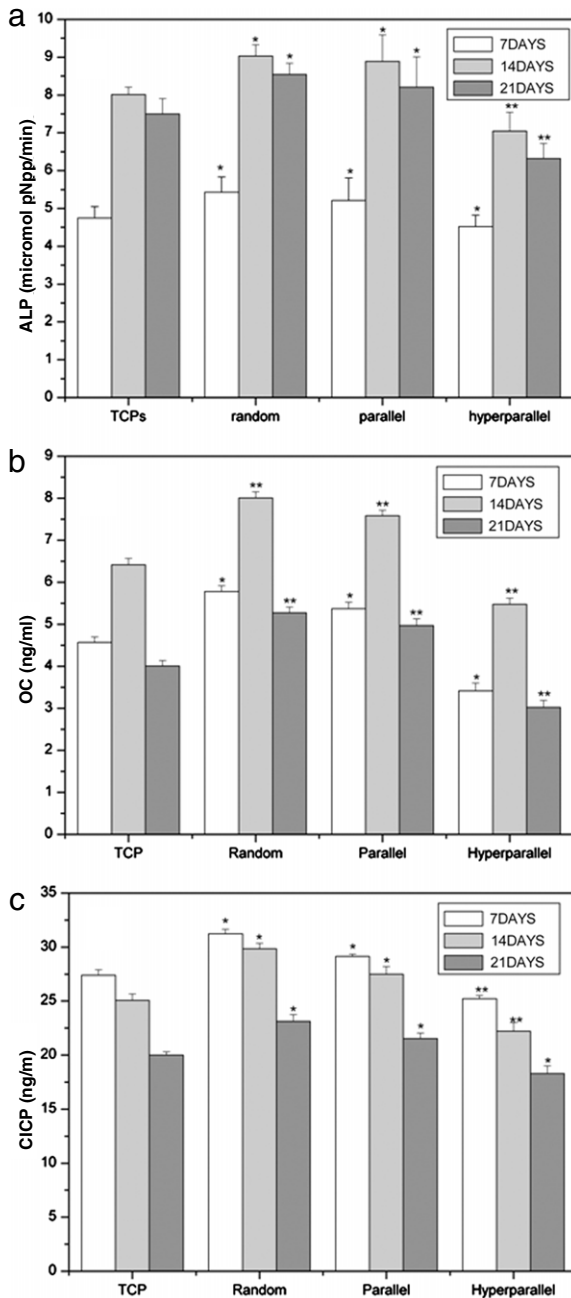
Fig. 11 – Alkaline phosphatase (ALP) activity, Collagen I (Col I) production and osteocalcin (OC) production of MG63 cells on nano-fibrous scaffolds with different topographies after 7, 14 and 21 days of culture (∗$p < 0.05$; ∗∗$p < 0.005$).

teoblast progenitor MG63 cells. Based on these observations, it could be deduced that the osteogenic differentiation of the osteoblast-like cells was down-regulated in response to the hot-stretched hyperparallel-aligned PLLA fibers that exhibited lower fiber array angles, thinner fiber diameters, larger fiber densities, higher hydrophobicity and higher crystallization. Because the ALP activity, Col I secretion and OC production of MG63 cells on the random PLLA nano-fibrous scaffolds were marginally higher (though not statistically higher) than those on the parallel PLLA nano-fibrous scaffolds, it only can be concluded that fiber orientation may indeed play a role in regulating cell responses, however, it is still uncertain about the extent basing on the results of the present work.

5. Conclusions

Electrospun hyperparallel-aligned nano-fibrous matrices have been applied in tissue engineering strategies recently. As such, orienting cells along fiber directions of scaffolds has been identified as a useful way to improve cell behavior in nerve, ligament and tendon regeneration. However, in this study, the culture results of MG63 cells on PLLA nano-fibrous scaffolds with different fiber orientations demonstrated that osteoblast-like cells preferred the random nano-fibrous scaffolds. Elongation and orientation of MG63 cells on the hyperparallel-aligned nano-fibers may deform the nucleus and subsequently affect gene expression. Moreover, randomly arranged nano-fibrous meshes exhibited larger fiber diameters, interfiber distances and elongation to break than the parallel-aligned meshes, which may have favored the infiltration and growth of cells in the former.

Acknowledgements

REFERENCES

Arima, Y., Iwata, H., 2007. Effect of wettability and surface functional groups on protein adsorption and cell adhesion using well-defined mixed self-assembled monolayers. Biomaterials 28, 3074–3082.

Badami, A.S., Kreke, M.R., Thompson, M.S., Riffle, J.S., Goldstein, A.S., 2006. Effect of fiber diameter on spreading, proliferation, and differentiation of osteoblastic cells on electrospun poly(lactic acid) substrates. Biomaterials 27, 596–606.

Baker, B.M., Mauck, R.L., 2007. The effect of nanofiber alignment on the maturation of engineered meniscus constructs. Biomaterials 28, 1967–1977.

Baker, B.M., Nathan, A.S., Gee, A.O., Mauck, R.L., 2010. The influence of an aligned nanofibrous topography on human mesenchymal stem cell fibrochondrogenesis. Biomaterials 31, 6190–6200.

and OC is a marker of late osteoblastic differentiation (Ehara et al., 2003).

We found that the cells cultured on the hyperparallel PLLA nano-fibrous scaffolds displayed the lowest ALP activity and Col I and OC production, while the random and parallel PLLA nano-fibrous scaffolds supported higher ALP activity, Col I secretion and OC production than the control group at 7, 14 and 21 days co-culture. These results suggested that electrospun PLLA nano-fibers including either random alignment or parallel alignment facilitated osteogenic differentiation of the os-

Barnes, C.P., Sell, S.A., Boland, E.D., Simpson, D.G., Bowlin, G.L., 2007. Nanofiber technology: designing the next generation of tissue engineering scaffolds. Adv. Drug. Deliv. Rev. 59, 1413–1433.

Bashur, C.A., Dahlgren, L.A., Goldstein, A.S., 2006. Effect of fiber diameter and orientation on fibroblast morphology and proliferation on electrospun poly(D, L-lactic-coglycolic acid) meshes. Biomaterials 27, 5681–5688.

Boanini, E., Torricelli, P., Gazzano, M., Giardino, R., Bigi, A., 2006. Nanocomposites of hydroxyapatite with aspartic acid and glutamic acid and their interaction with osteoblast-like cells. Biomaterials 27, 4428–4433.

Chen, C.S., Mrksich, M., Huang, S., Whitesides, G.M., Ingber, D.E., 1997. Geometric control of cell life and death. Science. 276, 1425–1428.

Chen, M., Patra, P.K., Warner, S.B., Bhowmick, S., 2007. Role of fiber diameter in adhesion and proliferation of NIH 3T3 fibroblast on electrospun polycaprolactone scaffolds. Tissue Eng. 13, 579–587.

Chew, S.Y., Mi, R.F., Hoke, A., Leong, K.W., 2008. The effect of the alignment of electrospun fibrous scaffolds on Schwann cell maturation. Biomaterials 29, 653–661.

Christopherson, G.T., Song, H., Mao, H.Q., 2009. The influence of fiber diameter of electrospun substrates on neural stem cell differentiation and proliferation. Biomaterials 30, 556–564.

Doshi, J., Reneker, D.H., 1995. Electrospinning process and applications of electrospun fibers. J. Electrostat. 35, 151–160.

Ehara, A., Ogata, K., Imazato, S., Ebisu, S., Nakano, T., Umakoshi, Y., 2003. Effects of a-TCP and TetCP on MC3T3-E1 proliferation, differentiation and mineralization. Biomaterials 24, 831–836.

Gang, S., Xiao, P.Y., Fang, M., Xiao, Y.H., Guo, Q.C., Xu, L.D., Seung, K.R., 2007. Poly-L-lactic acid/hydroxyapatite hybrid membrane for bone tissue regeneration. J. Biomed Mater. Res. A. 82, 445–454.

Guilak, F., Cohen, D.M., Estes, B.T., Gimble, J.M., Liedtke, W., Chen, C.S, 2009. Control of stem cell fate by physical interactions with the extracellular matrix. Cell. Stem. Cell. 5, 17–26.

He, L., Liao, S., Quan, D., Ma, K., Chan, C., Ramakrishna, S., Lu, J., 2010. Synergistic effects of electrospun PLLA fiber dimension and pattern on neonatal mouse cerebellum C17.2 stem cells. Acta Biomaterialia 6, 2960–2969.

Katta, P., Alessandro, M., Ramsier, R.D., Chase, G.G., 2004. Continuous electrospinning of aligned polymer nanofibers onto a wire drum collector. Nano Lett. 4 (11), 2215–2218.

Khang, D., Sato, M., Price, R.L., Ribbe, A.E., Webster, T.J., 2006. Selective adhesion and mineral deposition by osteoblasts on carbon nanofiber patterns. Int. J. Nanomedicine 1, 65–72.

Kim, H.W., Lee, H.H., Chun, G.S., 2008. Bioactivity and osteoblast responses of novel biomedical nanocomposites of bioactive glass nanofiber filled poly(lactic acid). J. Biomed. Mater. Res. A. 85, 651–663.

Li, C., Vepari, C., Jin, H.J., Kim, H.J., Kaplan, D.L., 2006. Electrospun silk-BMP-2 scaffolds for bone tissue engineering. Biomaterials 27, 3115–3124.

Li, Z., Yang, M., Xie, B., Feng, J., Huang, R., 2003. In-situ microfiber reinforced composite based on PET and PE via slit die extrusion and hot stretching: Influences of hot stretching ratio on morphology and tensile Properties at a fixed composition. Polym. Eng. Sci. 43, 615–628.

Ling, X., Spruiell, J.E., 2006. Analysis of the complex thermal behavior of poly(L-lactic acid) film. I. Samples crystallized from the glassy state. J. Polym. Sci. B Polym. Phys. 44, 3200–3214.

Liu, Y., Ji, Y., Ghosh, K., Clark, R.A.F., Huang, L., Rafailovich, M.H., 2009. Effects of fiber orientation and diameter on the behavior

of human dermal fibroblasts on electrospun PMMA scaffolds. J. Biomed. Mater. Res. A 90, 1092–1106.

Lorenzo, M., Ruud, L., Jan, B., Joost, R.W., Clemens, A.B., 2006. Fiber diameter and texture of electrospun PEOT/PBT scaffolds influence human mesenchymal stem cell proliferation and morphology, and the release of incorporated compounds. Biomaterials 27, 4911–4922.

Lowery, J.L., Datta, N., Rutledge, G.C., 2010. Effect of fiber diameter, pore size and seeding method on growth of human dermal fibroblasts in electrospun poly(e-caprolactone) fibrous mats. Biomaterials 31, 491–504.

Malaval, L., Liu, F., Roche, P., Aubin, J.E., 1999. Kinetics of osteoprogenitor proliferation and osteoblast differentiation in vitro. J. Cell. Biochem. 74, 616–627.

Mammoto, A., Ingber, D.E., 2010. Cytoskeletal control of growth and cell fate switching. Curr. Opin. Cell. biol. 21, 864–870.

Matsuzaka, K., Walboomers, X.F., Ruijter, J.E., Jansen, J.A., 1999. The effect of poly L-lactic acid with parallel surface microgroove on osteoblast-like cells in vitro. Biomaterials 20, 1293–1301.

Moroni, L., Licht, R., de Boer, J., de Wijn, J.R., van Blitterswijk, C.A., 2006. Fiber diameter and texture of electrospun PEOT/PBT scaffolds influence human mesenchymal stem cell proliferation and morphology, and the release of incorporated compounds. Biomaterials 27, 4911–4922.

Roskelley, C.D., Desprez, P.Y., Bissell, M.J., 1994. Extracellular matrix-dependent tissue-specific gene expression in mammary epithelial cells requires both physical and biochemical transduction. Proc. Natl. Acad. Sci. USA. 91, 12378–12382.

Sangsanoh, P., Waleetorncheepsawat, S., Suwantong, O., Wutticharoenmongkol, P., Weeranantanapan, O., Chuenjitbuntaworn, B., Poonlarp, C., Prasit, P., Pitt, S., 2007. In vitro biocompatibility of Schwann cells on surfaces of biocompatible polymeric electrospun fibrous and solution-cast film scaffolds. Biomacromolecules 8, 1587–1594.

Schnell, E., Klinkhammer, K., Balzer, S., Brook, G., Klee, D., Dalton, P., Mey, J., 2007. Guidance of glial cell migration and axonal growth on electrospun nanofibers of poly-ε-caprolactone and a collagen/poly-ε-caprolactone blend. Biomaterials 28, 3012–3025.

Sundaray, B., Subramanian, V., Natarajan, T.S., Xiang, R.Z., Chang, C.C., Fann, W.S., 2006. Electrospinning of continuous aligned polymer fibers. Appl. Phys. Lett. 47, 4901–4904.

Watt, F.M., Jordan, P.W., O'Neill, C.H., 1988. Cell shape controls terminal differentiation of human epidermal keratinocytes. Proc. Natl. Acad. Sci. USA. 85, 5576–5580.

Woo, K.M., Jun, J.H., Chen, V.J., Seo, J., Baek, J.H., Ryoo, H.M., Kim, G.S., Somerman, M.J., Ma, P.X., 2007. Nano-fibrous scaffolding promotes osteoblast differentiation and biomineralization. Biomaterials 28, 335–343.

Wutticharoenmongkol, P., Pavasant, P., Supaphol, P., 2007. Osteoblastic phenotype expression of MC3T3-E1 cultured on electrospun polycaprolactone fiber mats filled with hydroxyapatite nanoparticles. Biomacromolecules 8, 2602–2610.

Zhu, B., Lu, Q., Yin, J., Hu, J., Wang, Z., 2005. Alignment of osteoblast-like cells and cell-produced collagen matrix induced by nanogrooves. Tissue Eng. 11, 825–834.

Zinger, O., Zhao, G., Schwartz, Z., Simpson, J., Wieland, M., Landolt, D., Barbara, B., 2005. Differential regulation of osteoblasts by substrate microstructural features. Biomaterials 26, 1837–1847.

Zong, X., Kim, K., Fang, D., Ran, S., Hsiao, B.S., Chu, B., 2002. Structure and process relationship of electrospun bioabsorbable nanofiber membranes. Polymer 43, 4403–4412.